Eur. Phys. J. C (2020) 80:526
https://doi.org/10.1140/epjc/s10052-020-8099-z

THE EUROPEAN PHYSICAL JOURNAL C

Regular Article - Theoretical Physics

Bottomonium spectrum with a Dirac potential model in the momentum space

David Molina[1,4,a], **Maurizio De Sanctis**[1,b], **César Fernández-Ramírez**[2,c], **Elena Santopinto**[3,d]

[1] Universidad Nacional de Colombia, Bogotá 111321, Colombia
[2] Instituto de Ciencias Nucleares, Universidad Nacional Autónoma de México, Mexico 04510, Mexico
[3] INFN, Sezione di Genova, via Dodecaneso 33, 16146 Genova, Italy
[4] Corporación Universitaria Minuto de Dios, Bogotá 111021, Colombia

Received: 18 April 2020 / Accepted: 29 May 2020 / Published online: 12 June 2020

Abstract We study the bottomonium spectrum using a relativistic potential model in the momentum space. This model is based on a complete one gluon exchange interaction with a momentum dependent screening factor to account for the effects due to virtual pair creation that appear close to the decay thresholds. The overall model does not make use of nonrelativistic approximations. We fit well established bottomonium states below the open bottom threshold and predict the rest of the spectrum up to ≈ 11200 MeV and $J^{PC} = 3^{--}$. Uncertainties are treated rigorously and propagated in full to the parameters of the model using a Monte Carlo to identify if which deviations from experimental data can be absorbed into the statistical uncertainties of the models and which can be related to physics beyond the $b\bar{b}$ picture, guiding future research. We get a good description of the spectrum, in particular the Belle measurement of the $\eta_b(2S)$ state and the $\Upsilon(10860)$ and $\chi_b(3P)$ resonances.

1 Introduction

The heavy quark meson sector constitutes a major piece of information on the nonperturbative regime of the strong interaction. In particular, a lot of experimental information has been gathered on the bottomonium spectrum during the last years thanks to ATLAS, BaBar, Belle, BESIII, CLEO, CMS, D0, and LHCb collaborations [1–12] and further results are expected in the near future during the Belle II run [13,14] and after the CMS and LHCb upgrades [15,16]. Theory work has preceded and followed through the experimental effort [17–21] in the form of Lattice QCD computations [22–33], Dyson–Schwinger–Bethe–Salpeter equations [34–40], effectives Hamiltonians reduced from QCD [41,42] and potential quark models [43–56]. In this paper we develop a relativistic quark model for bottomonia based on a complete one gluon exchange. The approach is completely relativistic and does not rely on nonrelativistic approximations. In this way the standard spin–orbit, spin–spin, and tensor interactions are automatically included. We also incorporate a relativistic scalar interaction and a momentum dependent screening factor to account for the effects due to virtual pair creation that appear close to the decay thresholds. All the calculations are performed in the momentum space. The same model was successfully applied to reproduce the charmonium spectrum in Ref. [57] which we refer the reader to for technicalities. We fit the model to all the known states of each J^{PC} below the $B\bar{B}$ threshold except for the recently measured $\chi_{b1}(3P)$ and $\chi_{b2}(3P)$ which we prefer to predict in order to gain insight on their nature and the $\eta_b(2S)$ which we exclude of our fit owing to the disagreement between CLEO [58] and Belle [59] measurements. We perform a rigorous error estimation that allows us to assess if the inclusion of a new effect in the phenomenological model is necessary or not, and we compute the parameter correlations which provide insight on how independent are the different pieces of the model among them. A full error analyses is mandatory to identify which deviations from experimental data can be absorbed into the statistical uncertainties of the models and which can be related to physics beyond the $b\bar{b}$ picture, guiding future research.

The paper is organized as follows: in Sect. 2 we provide the relativistic quark model and the employed solution method; in Sect. 3 we describe the fitting procedure as well as the statistical method used to compute the uncertainties; in Sect. 4 we report the computed bottomonium spectrum up

[a] e-mail: djmolinab@unal.edu.co (corresponding author)
[b] e-mail: mdesanctis@unal.edu.co
[c] e-mail: cesar.fernandez@nucleares.unam.mx
[d] e-mail: santopinto@ge.infn.it

to $J^{PC} = 3^{--}$ and ≈ 11200 MeV as well as the comparison to the available experimental information. We obtain a very good description of both fitted and nonfitted bottomonia and also predict many unobserved states; Sect. 5 summarizes the conclusions.

2 Model and relativistic equation

2.1 Hamiltonian model

We apply to bottomonia the same model developed in [57] for charmonia. The total interaction Hamiltonian of this model is given by the sum of a vector ($\bar{\mathcal{H}}^{(v)}$) and a scalar ($\bar{\mathcal{H}}^{(s)}$) term. In the momentum space, it has the form:

$$\bar{\mathcal{H}}_{\rm int}(\mathbf{p}_b, \mathbf{p}_a) = \bar{\mathcal{H}}^{(v)}(\mathbf{p}_b, \mathbf{p}_a) + \bar{\mathcal{H}}^{(s)}(\mathbf{p}_b, \mathbf{p}_a), \tag{1}$$

where $\mathbf{p}_a$ and $\mathbf{p}_b$ represent the three-momenta of both quark and antiquark in the center of mass of the bottomonium system. In more detail, the vector interaction is constructed in the Coulomb gauge taking into account the whole one gluon exchange contribution. We have:

$$\bar{\mathcal{H}}^{(v)}(\mathbf{p}_b, \mathbf{p}_a) = V^{(v)}(\mathbf{q}) \left[J_1^0\, J_2^0 \left(1 - \frac{(\Delta E)^2}{Q^2}\right) - \mathbf{J}_1 \cdot \mathbf{J}_2 \left(1 + \frac{(\Delta E)^2}{Q^2}\right)\right], \tag{2}$$

The *effective potential function* $V^{(v)}(\mathbf{q})$ will be introduced and discussed in the following Eq. (7a). Furthermore,

$$J_i^\mu = J_i^\mu(\sigma_i; \mathbf{p}_b, \mathbf{p}_a) = \bar{u}(\mathbf{p}_{ib}, \sigma_i)\gamma_i^\mu u(\mathbf{p}_{ia}, \sigma_i), \tag{3}$$

represents the standard Dirac four-current of the quarks, $\boldsymbol{\sigma}_i$ stands for the Pauli matrices, and γ_i^μ are the gamma matrices, where $i = 1, 2$ is the particle label. We also introduce the quark on-shell energy difference

$$\Delta E = E(\mathbf{p}_b) - E(\mathbf{p}_a), \tag{4}$$

(being $E(\mathbf{p}) = \sqrt{\mathbf{p}^2 + m^2}$) and the squared (positive) four momentum transfer

$$Q^2 = \mathbf{q}^2 - (\Delta E)^2. \tag{5}$$

where $\mathbf{q} = \mathbf{p}_b - \mathbf{p}_a$ represents the three momentum transfer. The factors $1 \pm \frac{(\Delta E)^2}{Q^2}$ give the retardation contributions in the Coulomb gauge. Analogously, the scalar interaction is defined as

$$\bar{\mathcal{H}}^{(s)}(\mathbf{p}_b, \mathbf{p}_a) = V^{(s)}(\mathbf{q})\, I_1\, I_2, \tag{6}$$

where I_i is a scalar vertex and $V^{(s)}(\mathbf{q})$ is the scalar effective potential function of the following Eq. (7b). Finally, the vector and the scalar effective potentials functions have the following form:

$$V^{(v)}(\mathbf{q}) = -\frac{4}{3}\frac{\alpha_{st}}{\mathbf{q}^2} + \beta_v \frac{3b^2 - \mathbf{q}^2}{(\mathbf{q}^2 + b^2)^3}, \tag{7a}$$

$$V^{(s)}(\mathbf{q}) = A + \beta_s \frac{3b^2 - \mathbf{q}^2}{(\mathbf{q}^2 + b^2)^3}. \tag{7b}$$

The first term of Eq. (7a) represents a standard vector interaction, mediated by a massless gluon; α_{st} is the effective strong coupling constant. When inserted in Eq. (2), the complete Coulomb gauge relativistic interaction (with the color factor 4/3) is obtained. The second term of Eq. (7a) represents a regularized confining interaction corresponding to a linear term in the coordinate space, as shown in Ref. [57], in which β_v corresponds to the vector confinement strength. As for the scalar potential function given by, Eq. (7b) we note that it contains a phenomenological constant term A plus a β_s term which corresponds to the scalar confinement strength. In both vector and scalar confining terms the regularization parameter b has been introduced to avoid the divergence when $|\mathbf{q}| \to 0$.

With the definitions given above, the complete interaction Hamiltonian of Eq. (1) can be straightforwardly constructed. In any case, all the details have been given in the Appendix of Ref. [57].

As in [57] for charmonia, we use two different prescriptions for the scalar interaction:

$$\begin{cases} \text{potential I} \to \text{model using Eqs. (7) with } \beta_s = 0, \\ \text{potential II} \to \text{model using Eqs. (7) with } \beta_s \neq 0. \end{cases} \tag{8}$$

In this way we can check if the two forms of the scalar interaction (with or without the confinement term) have the same effect on the spectrum, as in the case of the charmonium system. Besides, in order to take into account the effects of the virtual [60,61] pair creation that appear close to the decays thresholds, we include a screening momentum dependent factor. Hence, the total Hamiltonian takes the final form

$$\begin{aligned} &\bar{\mathcal{H}}_{\rm int}(\mathbf{p}_b, \mathbf{p}_a) \to \mathcal{H}_{\rm int}(\mathbf{p}_b, \mathbf{p}_a) \\ &= F_s(p_b)\bar{\mathcal{H}}_{\rm int}(\mathbf{p}_b, \mathbf{p}_a)F_s(p_a), \end{aligned} \tag{9}$$

where the screening factors $F_s(p)$ with p_a or p_b is defined as

$$F_s(p) = \frac{1 + k_s}{k_s + \exp\left(p^2/p_s^2\right)}. \tag{10}$$

Where p_s and k_s are others parameter of the model. In this way, the model, with potential I and potential II, depends on seven and eight parameters, respectively (see Table 2).

2.2 Relativistic equation and solution method

The relativistic equation we use has been obtained performing a three dimensional reduction of the Bethe–Salpeter equation and keeping only the contributions of the positive energy Dirac spinors [57]. In the center of mass of the $b\bar{b}$ system, the relativistic integral equation takes the form

$$[K(\mathbf{p_b}) + M_0]\Psi(\mathbf{p}_b) + \int d^3p_a \mathcal{H}_{\rm int}(\mathbf{p}_b, \mathbf{p}_a)\Psi(\mathbf{p}_a) = M\,\Psi(\mathbf{p}_b), \tag{11}$$

where we have introduced the relativistic energy

$$K(\mathbf{p}) = 2\sqrt{\mathbf{p}^2 + m^2}, \tag{12}$$

and M_0 represents the phenomenological zero point energy of the spectrum, M is the resonance mass (i.e. the eigenvalue of the integral equation) and $\Psi(\mathbf{p})$ is the resonance wave function. The wave function $\Psi_{n,\{\nu\}}(\mathbf{p})$ ($\{\nu\} = L, S, J$) can be written as

$$\Psi_{n,\{\nu\}}(\mathbf{p}) = R_{n,L}(p;\bar{p})\left[Y_L(\hat{p}) \otimes \chi_S\right]_{J,M_J}, \tag{13}$$

where $R_{n,L}(p;\bar{p})$ corresponds to the radial function in the momentum space with n the principal quantum number, $\bar{p}$ the variational parameter (with dimensions of momentum), $Y_{L,M_L}(\hat{p})$ are the spherical harmonics, and χ_{S,M_S} is the spin function. To solve Eq. (11) we use the variational method. As trial functions we use a combination of a finite subset of three dimensional harmonic oscillators. Hence, we can write the Hamiltonian matrix as

$$M_{\{\nu\},n_b,n_a} = M_0\delta_{n_b,n_a} + \int d^3p\, \Psi^{\dagger}_{n_b,\{\nu\}}(\mathbf{p})K(\mathbf{p})\Psi_{n_a,\{\nu\}}(\mathbf{p}) + \int d^3p_b\, d^3p_a \Psi^{\dagger}_{n_b,\{\nu\}}(\mathbf{p_b})\mathcal{H}_{\rm int}(\mathbf{p}_b,\mathbf{p}_a)\Psi_{n_a,\{\nu\}}(\mathbf{p_a}). \tag{14}$$

The eigenvalues and the eigenstates are found through the variational method, diagonalizing and minimizing the $M_{\{\nu\},n_b,n_a}$ matrix in Eq. (14) [57,62]. The angular part is solved analytically and the radial part numerically. The details can be found in the Appendix of Ref. [57].

3 Parameter determination

To determine the values of the parameters, the uncertainties, and the theoretical bottomonium spectrum we fit the experimental masses given in Table 1, i.e. all the known states of each J^{PC} below the $B\bar{B}$ threshold except for the recently measured $\chi_{b1}(3P)$ and $\chi_{b2}(3P)$ which we try to predict in order to gain insight on their nature and the $\eta_b(2S)$ which we prefer to exclude of our fit owing to the disagreement between CLEO and Belle masses [51]. From CLEO data a mass of $9974.6 \pm 2.3 \pm 2.1$ MeV [58] was obtained while Belle measures $9999.0 \pm 3.5^{+2.8}_{-1.9}$ MeV [59]. BABAR reports a range value between 9974 and 10,015 MeV [63]. The PDG favors the Belle measurement [12], therefore we show this experimental value in Table 1 and Figs. 1 and 2. To perform the fits and the error analyses we use the bootstrap technique [64–67] and proceed as follows:

1. We randomly choose values for the masses of the resonances by sampling a Gaussian distribution according to their uncertainties (systematic and statistical summed in quadrature), obtaining a resampled bottomonium spectrum;
2. We use the least-squares method to minimize the squared distance

$$d^2 = \sum_i \left(E_i^{th} - M_i\right)^2, \tag{15}$$

where M_i are the resampled experimental bottomonia, i.e. the states 0^{-+} ($\eta_b(1S)$); 1^{--} ($\Upsilon(1S)$, $\Upsilon(2S)$, $\Upsilon(3S)$); 0^{++} ($\chi_{b0}(1S)$, $\chi_{b0}(2S)$); 1^{+-} ($h_b(1P), h_b(2P)$); 1^{++} ($\chi_{b1}(1P)$, $\chi_{b2}(2S)$); 2^{--} ($\Upsilon(1D)$) y 2^{++} ($\chi_{b2}(1P)$, $\chi_{b2}(2S)$). The E_i^{th} represents the theoretical states calculated by solving the eigenvalue Eq. (14) with potentials I and II. The fit is performed using MINUIT [68].

This procedure is repeated 1000 times in order to obtain enough statistics to compute the expected values of the parameters as well as their uncertainties at a 1σ (68%) confidence level (CL). The expected value of the parameters (Table 2) are computed as the mean value of the 1000 samples. The uncertainties are obtained as the the differences between the mean value and the highest and lowest masses of the best 68% of the fits. Hence, our uncertainties can be asymmetric. Once the parameters have been determined, we can compute the bottomonium spectrum and the associated uncertainties (Table 1). We find an excellent agreement between theory and fitted states within uncertainties. We note that the values of the common parameters of the two potentials are very similar. These results show that, unlike for charmonia, the scalar confinement term of the interaction does not seem to be relevant in the bottomonia description. To gain further insight on this issue we compute the correlation matrices, Tables 3 and 4, for potentials I and II, respectively.

For potential I (Table 3) we find a strong correlation between the parameters of the vector interaction (α_s and β_v) and the scalar interaction parameter A, which indicates that vector and scalar interactions are physically correlated in this model. The screening parameter p_s is weakly correlated with the vector interaction parameters but strongly correlated with

Table 1 Fitted bottomonia for potentials I and II compared to the PDG values; n stands for the principal quantum number, L for the orbital angular momentum, J for the total angular momentum, and S for the spin. The statistical and systematic errors have been added in quadrature for the bootstrap technique

Name	$n\,^{2S+1}L_J$	Masses (MeV)		
		Potential I	Potential II	Experiment
η_b	$1\,^1S_0$	9402^{+27}_{-24}	9404^{+19}_{-14}	9399.0 ± 2.3
$\Upsilon(1S)$	$1\,^3S_1$	9455^{+21}_{-23}	9454^{+19}_{-16}	9460.30 ± 0.26
$\chi_{b0}(1P)$	$1\,^3P_0$	9856^{+22}_{-20}	9858^{+14}_{-19}	$9859.44 \pm 0.42 \pm 0.31$
$\chi_{b1}(1P)$	$1\,^3P_1$	9894^{+17}_{-15}	9893^{+9}_{-11}	$9892.78 \pm 0.26 \pm 0.31$
$h_b(1P)$	$1\,^1P_1$	9902^{+17}_{-16}	9901^{+9}_{-10}	9899.3 ± 0.8
$\chi_{b2}(1P)$	$1\,^3P_2$	9927^{+15}_{-17}	9923^{+13}_{-14}	$9912.21 \pm 0.26 \pm 0.31$
$\Upsilon(2S)$	$2\,^3S_1$	$10{,}017^{+20}_{-19}$	$10{,}016^{+17}_{-15}$	$10{,}023.26 \pm 0.31$
$\Upsilon(1D)$	$1\,^3D_2$	$10{,}151^{+13}_{-19}$	$10{,}149^{+16}_{-14}$	$10{,}163.7 \pm 1.4$
$\chi_{b0}(2P)$	$2\,^3P_0$	$10{,}232^{+18}_{-16}$	$10{,}233^{+12}_{-13}$	$10{,}232.5 \pm 0.4 \pm 0.5$
$\chi_{b1}(2P)$	$2\,^3P_1$	$10{,}253^{+14}_{-15}$	$10{,}254^{+7}_{-11}$	$10{,}255.46 \pm 0.22 \pm 0.50$
$h_b(2P)$	$2\,^1P_1$	$10{,}257^{+14}_{-15}$	$10{,}259^{+8}_{-10}$	$10{,}259.8 \pm 0.5 \pm 1.1$
$\chi_{b2}(2P)$	$2\,^3P_2$	$10{,}274^{+13}_{-15}$	$10{,}274^{+11}_{-12}$	$10{,}268.65 \pm 0.22 \pm 0.50$
$\Upsilon(3S)$	$3\,^3S_1$	$10{,}361 \pm 25$	$10{,}364 \pm 14$	$10{,}355.2 \pm 0.5$

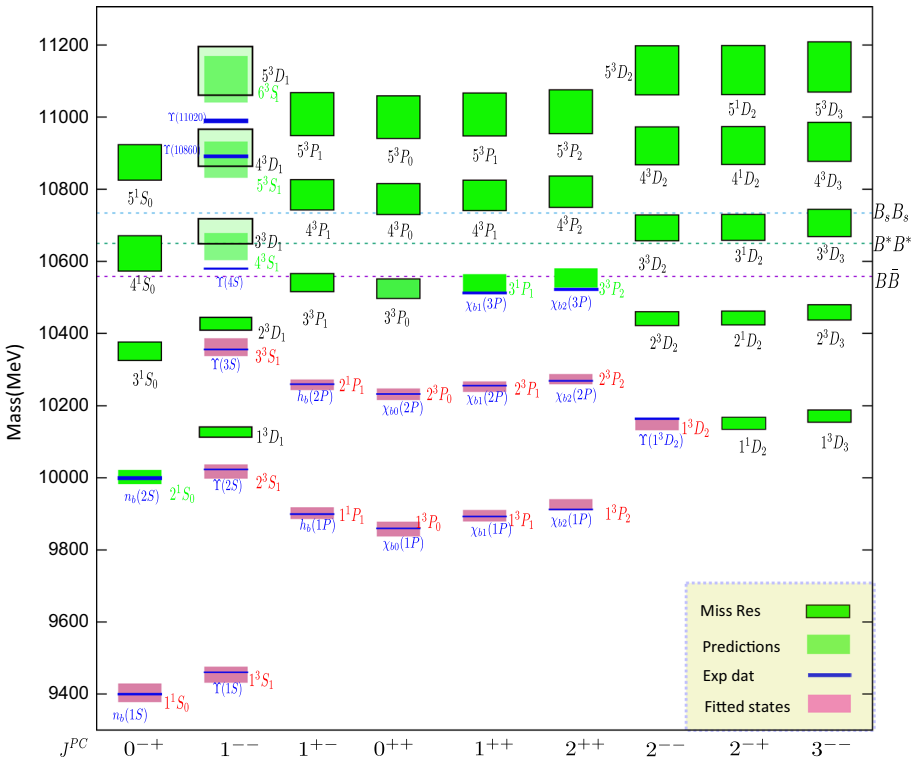

Fig. 1 Bottomonium spectrum computed with potential I. The blue boxes represent the experimental states with their error bands, the purple ones provide the computation of the fitted states. The green boxes represent the predictions of the model and, in particular, those with black edges correspond to missing resonances. For simplicity we only include the names of the experimentally known states

the scalar interaction ones. For potential II, we have the additional parameter β_s. In this potential, the parameters are less correlated as shown in Table 4 with one exception, the additional scalar interaction parameter β_s is noticeble correlated with the vector interaction parameter β_v. Consequently, we find a significant correlation between the confinement terms of the vector and the scalar interactions. The parameter p_s of the screening factors is weakly correlated with the other parameters of the interactions except with the phenomenological parameter A in the scalar interaction. This sizeable correlation highlights how the screening factor impacts more on the scalar interaction.

Using the values obtained in the fitting procedure we plot the screening function $F_s(p)$ in Fig. 3 for the two potentials.

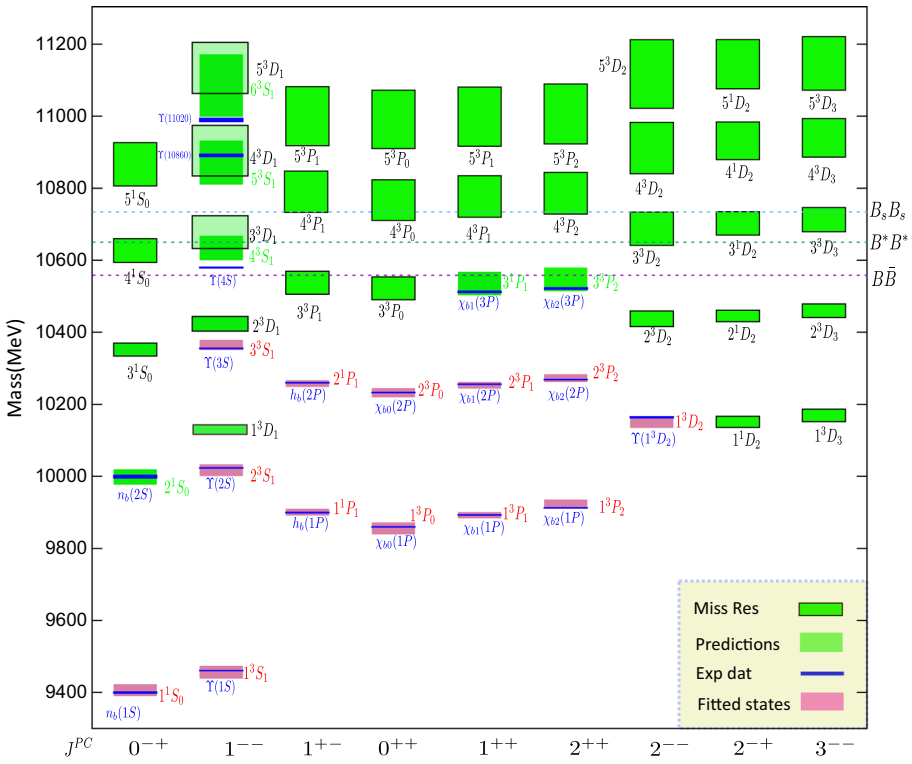

Fig. 2 Bottomonium spectrum computed with potential II. Same conventions as in Fig. 1

Table 2 Fit parameters for both potentials. Error bars are reported at 1σ (68%) CL and take into account all the correlations among the parameters

Parameter	Potential I	Potential II
m (GeV)	$4.52^{+0.13}_{-0.13}$	$4.51^{+0.08}_{-0.09}$
M_0 (GeV)	$0.48^{+0.33}_{-0.27}$	0.47 ± 0.2
α_{st}	$0.39^{+0.09}_{-0.10}$	$0.37^{+0.10}_{-0.10}$
β_v (GeV^2)	$0.018^{+0.004}_{-0.001}$	$0.017^{+0.003}_{-0.003}$
k_s	98^{+22}_{-12}	100^{+29}_{-20}
p_s (GeV)	$1.55^{+0.23}_{-0.20}$	$1.56^{+0.23}_{-0.21}$
A (GeV^{-2})	0.0011 ± 0.0010	-0.0013 ± 0.0013
β_s (GeV^2)	0 (fixed)	$0.090^{+0.002}_{-0.002}$

Table 3 Correlation matrix for the parameters of potential I

	m	M_0	α_{st}	β_v	k_s	p_s	A
m	1						
M_0	−0.89	1					
α_{st}	0.13	0.30	1				
β_v	−0.08	−0.36	−0.87	1			
k_s	−0.03	0.01	−0.09	0.03	1		
p_s	0.09	−0.09	−0.07	0.08	0.02	1	
A	−0.18	−0.10	−0.68	0.46	−0.12	−0.55	1

Table 4 Correlation matrix for the parameters of potential II

	m	M_0	α_{st}	β_v	k_s	p_s	A	β_s
m	1							
M_0	−0.76	1						
α_{st}	0.53	0.14	1					
β_v	−0.26	−0.15	−0.58	1				
k_s	0.34	−0.29	0.06	−0.04	1			
p_s	0.13	−0.13	−0.05	0.03	0.36	1		
A	0.42	−0.05	0.52	−0.32	0.48	0.77	1	
β_s	−0.21	0.01	−0.31	−0.57	−0.03	0.07	−0.07	1

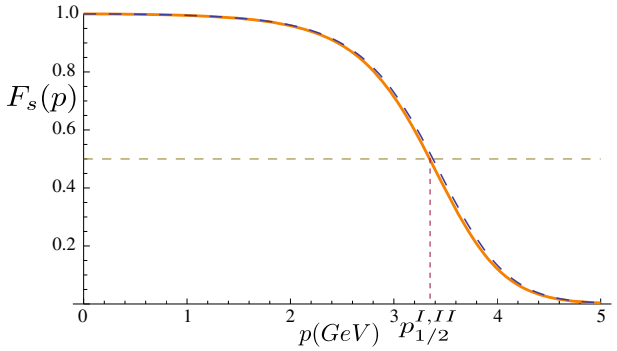

Fig. 3 Screening function for potentials I (dashed blue) and II (solid orange). For k_s and p_s we use the central values in Table 2. We highlight the values of the screening momenta $p^{\rm I}_{1/2}$ (potential I) and $p^{\rm II}_{1/2}$ (potential II) introduced in [57]

As mentioned above we introduce the screening momenta $p^{\rm j}_{1/2}$ (j = I, II labels potentials I and II) which are given by $F_s(p^{\rm j}_{1/2}) = 1/2$ (we recall that $F_s(0) = 1$). Through the fitting values, we find $p^{\rm I}_{1/2} = 3.38$ GeV and $p^{\rm II}_{1/2} = 3.34$ GeV. These values correspond to the screening kinetic energy

$$\bar{E}^{\rm j} = 2\sqrt{m^2 + \left(p^{\rm j}_{1/2}\right)^2}, \tag{16}$$

which amount to $\bar{E}^{\rm I} = 11.281$ GeV for potential I and $\bar{E}^{\rm II} = 11.260$ GeV for potential II. This result show that the screening effect is active above the open bottom threshold as in charmonia. Nevertheless, due to the high values of $\bar{E}^{\rm I,II}$, we find that the screening effect is less relevant for the low-lying part of the bottomonium spectrum than for charmonia [57].

4 Bottomonium spectrum

Using the relativistic model interaction, with either potential I or II, we obtain the bottomonium spectrum. Through the bootstrap method, the errors in the fitted states are carried in full to the computed uncertainties in the parameters and to the spectrum. We provide the computed spectrum in Tables 1 (fitted states) and 5 (predicted states). The computed and the experimental spectra are compared in Figs. 1 (potential I) and 2 (potential II). In general, the spectrum is reproduced by the model within the experimental uncertainties.

We note that the parameters obtained with both potentials are very similar, leading to closely akin spectra. This result shows that the confining part of the scalar potential does not impact the bottomonium spectrum. However, the presence of the scalar interaction is necessary for an optimum fit, i.e. the parameter A contribution in Eq. (7b). In what follows we look into the states that were not included in the fit as well as the predicted higher-lying spectrum.

As a general remark, we note that the obtained spectrum is similar to the results of nonrelativistic and semirelativistic calculations [43–56]. In this concern, it can be argued that the high value of the bottom quark mass tends to reduce the relativistic effects with respect, for example, to the charmonium case. But also, the values of the effective parameters of the nonrelativistic and semirelativistic calculations can simulate some relativistic effects. Furthermore, the different dynamical details of the various models do not allow for straightforward and definitive conclusions about this point.

4.1 $\Upsilon(4S)$, $\Upsilon(10860)$ and $\Upsilon(11020)$

These resonances belong to the family with quantum numbers 1^{--}. They were discovered by means of e^+e^- collisions in the mid-eighties [70,71] and were more recently measured by the Belle collaboration [72]. The $\Upsilon(4S)$ is regarded as a 4^3S_1 state; its experimental mass is $M_{\Upsilon(4S)} = 10579.4 \pm 1.2$ MeV and is not well reproduced by either potential I or II. This resonance is generally considered as a $b\bar{b}$ state, but its mass is overestimated by models that make use of different approaches: e.g., the nonrelativistic model in Ref. [43] provides $M_{\Upsilon(4S)} \simeq 10630$ MeV, the semirelativistic model of Ref. [51] finds $M_{\Upsilon(4S)} = 10607$ MeV, and the non-

relativistic coupled channels model in Ref. [45] reports $M_{\Upsilon(4S)} = 10603$ MeV. Our computations provides approximately 10642 ± 40 MeV, with both potentials. This result is compatible with the other models, but far away from the experimental value, even when the uncertainties are taken into account. Consequently, our result combined with non-relativistic calculations suggest that there must be beyond the $q\bar{q}$ picture effects that need to be included to properly describe the state.

The $\Upsilon(10860)$ resonance is generally interpreted as a $\Upsilon(5^3S_1)$, e.g. in [43,45,49,51,52]. However, the theoretical calculations for the pion emission decay widths, to $\Upsilon(1S)$, $\Upsilon(2S)$ and $\Upsilon(3S)$ are two orders of magnitude [48] greater than the measurement [73] leading to different possible interpretations, such as that $\Upsilon(10860)$ is a mixing of a standard $\Upsilon(5S)$ with a P hybrid state [74], Finally, in Ref. [44] this state is interpreted as a $\Upsilon(6S)$, and, hence, the $\Upsilon(5S)$ becomes a missing resonance of the experimental spectrum In our model, this mass state can be reproduced as a $\Upsilon(5S)$ (5^3S_1) (see Table 5; Figs. 1 and 2) or as a 4^3D_1 state with both potentials. We do not find support the $\Upsilon(6S)$ interpretation. Actually, our predicted mean value mass, with $\Upsilon(5S)$, is only 5 (1) MeV away from the experimental value with potential I (II). Consequently, we identify this state as a $b\bar{b}$ with $\Upsilon(5S)$ quantum numbers. However, any final conclusion requires the explanation of the before mentioned pion emission decay widths which we leave for a future work.

Finally, the high excitation $\Upsilon(11020)$ state has been successfully described in standard calculations as a $b\bar{b}$ meson in a 6^3S_1 state. We recall, in particular, Refs. [50,51]. For completeness, we also mention that in Ref. [44] it is interpreted as a 7^3S_1 state. Our model gives a slightly higher mass value to the 6^3S_1 state, with either potential. Our results are similar to that of the relativized calculation of Ref. [43]. At the moment, no further conclusions can be drawn for this state within the present model.

4.2 $\chi_b(3P)$ states

The $\chi_b(3P)$ states have been the focus of several experimental collaborations during the last years. An estimation of the $\chi_b(3P)$ system *barycenter* (i.e. spin-weighted mass average of the $\chi_{b0}(3P)$, $\chi_{b1}(3P)$, and $\chi_{b2}(3P)$ states) was reported by ATLAS [1] and D0 [2] collaborations, yielding $10{,}530 \pm 5(stat) \pm 9(syst)$ MeV and $10551 \pm 14(stat) \pm 17(syst)$ MeV, respectively. More recently, two out of the three state masses were measured; $\chi_{b1}(3P)$ by the LHCb collaboration obtaining $10515.7^{+2.2}_{-3.9}(stat)^{+1.5}_{-2.1}(syst)$ MeV, and $\chi_{b1}(3P)$ and $\chi_{b2}(3P)$ by the CMS collaboration [7] yielding $10{,}513.42 \pm 0.41(stat) \pm 0.18(syst)$ MeV and $10{,}524.02 \pm 0.57(stat) \pm 0.18(syst)$ MeV, respectively. Several predictions of these states are available in the literature, employing different frameworks. For example, in Ref. [60] a mass of 10,524 MeV is predicted for the $\chi_{b1}(3P)$ state employing a screened potential; in Ref. [45], 10,517 MeV for the same state by means of a coupled channel calculation; and 10,580 MeV in the unquenched quark model [46]. All of the results overestimate the mass of $\chi_{b1}(3P)$. In our calculation (which porpously does not fit this state) we obtain $\simeq 10540 \pm 30$ MeV with both potentials whose central value also overestimates the mass of the state. When the uncertainties are taken into account, the experimental mass falls within our error bars and no indication of the need for additional physics is called for. This shows how important it is to perform a rigorous error estimation when performing a level-by-level comparison between theory and experiment, as differences that can be accounted by the error analyses can be mistaken by physics beyond the $b\bar{b}$ picture. Regarding $\chi_{b2}(3P)$, 10,532.4 MeV is obtained in Ref. [45] using the coupled channels formalism and 10,578 MeV under the unquenched quark model [46]. We obtain 10554^{+25}_{-28} and $10{,}557^{+22}_{-42}$ with potentials I and II, respectively. The CMS value falls well within our uncertainites for potential I and slightly out of them for potential II, although certainly within 2σ uncertainties. Hence, the individually measured $\chi_b(3P)$ states are well reproduced by our model. Finally, we obtain the barycenter mass $10{,}545^{+24}_{-27}$ MeV for potential I and $10{,}549^{+23}_{-41}$ MeV for potential II, both compatible with the previously quoted ATLAS and D0 estimations. Recalling that not all the individual states of the $\chi_{bJ}(3P)$ system have been measured, we provide in Tables 6 (potential I) and 7 (potential II) the $n = 1, 2, 3$ barycenter masses, given by [75,76]

$$\bar{M}_{nP} = \frac{M_{\chi_{b0}(nP)} + 3M_{\chi_{b1}(nP)} + 5M_{\chi_{b2}(nP)}}{9}, \tag{17}$$

along with the available experimental measurements and estimates from PDG values Given that both potentials produce similar spectra, the $\chi_b(nP)$ barycenters are very similar. In summary, we find a good agreement, within errors, between the models and the experimental barycenters.

Finally, we would like to mention that it has been theorized that some of the states in the $\chi_b(3P)$ system could be the bottomonia counterparts of the $X(3872)$ charmonium [47,77], i.e. states closely related to the opening if the $B\bar{B}$, $B\bar{B}^*$, and B_sB_s thresholds. Our results do not support such hypothesis, as the model reproduces the $\chi_b(3P)$ system within (large) uncertainties, contrary to the $X(3872)$ case which was overestimated using the same model [57], and whose description (both mass and width) calls for additional dynamics beyond the $c\bar{c}$ picture. Along the same ideas, according to Ref. [78], the $\chi_{b1}(4P)$ state could significantly couple to the $B\bar{B}^*$ and $B^*\bar{B}^*$ channels. The measurement of this particular state combined with the comparison to quark model calculations, like the one presented in this work, can provide insight on

Table 5 Predicted bottomonia for potentials I and II compared to the existing experimental masses with their corresponding uncertainties. Notation as in Table 1

Name	$n^{2S+1}L_J$	Mass (MeV)		
		Potential I	Potential II	Experiment
$\eta_b(2S)$	2^1S_0	10000^{+21}_{-17}	9999^{+20}_{-22}	$9999.0 \pm 3.5^{+2.8}_{-1.9}$[59]
–	1^1D_2	10153^{+14}_{-69}	10150^{+16}_{-14}	–
–	1^3D_1	10130^{+11}_{-17}	10128^{+14}_{-12}	–
–	1^3D_3	10173^{+15}_{-19}	10169 ± 17	–
–	2^1D_2	10445^{+17}_{-21}	10446^{+15}_{-16}	–
–	2^3D_1	10427^{+17}_{-19}	10429^{+14}_{-26}	–
–	2^3D_2	10443^{+17}_{-21}	10444^{+15}_{-28}	–
–	2^3D_3	10460^{+19}_{-23}	10461^{+18}_{-20}	–
$\eta_b(3S)$	3^1S_0	10351^{+26}_{-25}	10353^{+16}_{-19}	–
$h_b(3P)$	3^1P_1	10542^{+24}_{-26}	10546^{+23}_{-40}	–
$\chi_{b0}(3P)$	3^3P_0	10523^{+28}_{-26}	10528^{+25}_{-38}	–
$\chi_{b1}(3P)$	3^3P_1	10538^{+26}_{-27}	10541^{+24}_{-41}	$10515.7^{+2.2\,+1.5}_{-3.9\,-2.1}$ [69]
				$10513.42 \pm 0.41 \pm 0.18$ [7]
$\chi_{b2}(3P)$	3^3P_2	10554^{+25}_{-28}	10557^{+22}_{-42}	$10524.02 \pm 0.57 \pm 0.18$ [7]
–	3^3D_2	10697^{+33}_{-39}	10701^{+59}_{-32}	–
–	3^1D_2	10699^{+32}_{-39}	10702^{+32}_{-32}	–
–	3^3D_3	10711^{+34}_{-41}	10714^{+35}_{-32}	–
–	3^3D_1	10685^{+31}_{-37}	10689^{+33}_{-29}	–
$\eta_b(4S)$	4^1S_0	10635^{+37}_{-39}	10638^{+22}_{-44}	–
$h_b(4P)$	4^1P_1	10787^{+41}_{-43}	10792^{+43}_{-71}	–
$\chi_{b0}(4P)$	4^3P_0	10773^{+42}_{-44}	10779^{+43}_{-69}	–
$\chi_{b1}(4P)$	4^3P_1	10785^{+43}_{-42}	10790^{+44}_{-71}	–
$\chi_{b2}(4P)$	4^3P_2	10796^{+42}_{-45}	10801^{+43}_{-72}	–
–	4^3D_2	10926^{+49}_{-56}	10929^{+53}_{-89}	–
–	4^1D_2	10927^{+49}_{-56}	10930^{+53}_{-51}	–
–	4^3D_3	10937^{+51}_{-58}	10940^{+53}_{-54}	–
–	4^3D_1	10915^{+48}_{-54}	10920^{+52}_{-48}	–
$\Upsilon(4S)$	4^3S_1	10642^{+36}_{-39}	10646^{+21}_{-46}	10579.4 ± 1.2 [12]
$\eta_b(5P)$	5^1S_0	10878^{+47}_{-51}	10883^{+42}_{-78}	–
$h_b(5P)$	5^1P_1	11013^{+58}_{-61}	11018^{+62}_{-101}	–
$\chi_{b0}(5P)$	5^3P_0	11002^{+60}_{-59}	11008^{+62}_{-99}	–
$\chi_{b1}(5P)$	5^3P_1	11011^{+58}_{-61}	11017^{+63}_{-101}	–
$\chi_{b2}(5P)$	5^1P_2	11020^{+59}_{-63}	11025^{+63}_{-103}	–
–	5^3D_2	11137^{+65}_{-72}	11137^{+73}_{-116}	–
–	5^1D_2	11138^{+64}_{-72}	11138^{+73}_{-63}	–
–	5^3D_3	11146^{+66}_{-74}	11146^{+74}_{-74}	–
–	5^3D_1	11128^{+64}_{-70}	11129^{+72}_{-69}	–
$\Upsilon(10860)$	5^3S_1	10884^{+48}_{-53}	10889^{+43}_{-79}	$10889.9^{+3.2}_{-2.6}$ [12]
$\Upsilon(11020)$	6^3S_1	11107^{+62}_{-66}	11108^{+64}_{-107}	$10992.9^{+10.0}_{-3.1}$ [12]

Table 6 Theoretical results obtained, using Potential I, for the states $\chi_{bJ}(nP)$ compared with the available experimental data; $n = 1, 2, 3$ is the principal quantum number; $\bar{M}_n$ stands for the barycenter of the system for each n. The experimental states for $n = 1, 2$ are taken from Ref. [7]. The statistical and systematic errors of the experimental states have been summed in quadrature in order to obtain the errors of the experimental barycenter masses. The theoretical uncertainties of the barycenters were propagated from the parameters through the bootstrap technique

Theory: Potential I				Experimental		
n	1	2	3	1	2	3
$M_{\chi_{b0}(nP)}$(MeV)	9856^{+22}_{-20}	10232^{+18}_{-16}	10523^{+28}_{-26}	$9859.44 \pm 0.42 \pm 0.31$	$10232.5 \pm 0.4 \pm 0.5$	–
$M_{\chi_{b1}(nP)}$(MeV)	9894^{+17}_{-15}	10253^{+14}_{-15}	10538^{+26}_{-27}	$9892.78 \pm 0.26 \pm 0.31$	$10255.46 \pm 0.22 \pm 0.50$	$10512.1 \pm 2.1 \pm 0.9$ [12] $10513.42 \pm 0.41 \pm 0.18$ [7]
$M_{\chi_{b2}(nP)}$(MeV)	9927^{+15}_{-17}	10274^{+13}_{-15}	10554^{+25}_{-28}	$9912.21 \pm 0.26 \pm 0.31$	$10268.65 \pm 0.22 \pm 0.50$	$10524.02 \pm 0.57 \pm 0.18$ [7]
$\bar{M}_{nP}$(MeV)	9908 ± 15	10262^{+14}_{-15}	10545^{+24}_{-27}	9899.87 ± 0.27	10260.20 ± 0.36	$10530 \pm 5 \pm 9$ [1] $10551 \pm 14 \pm 17$ [2]

Table 7 Same as in Table 6 with the results given by Potential II

Theory: Potential II				Experimental		
n	1	2	3	1	2	3
$M_{\chi_{b0}(nP)}$(MeV)	9858^{+14}_{-19}	10233^{+12}_{-13}	10528^{+25}_{-38}	$9859.44 \pm 0.42 \pm 0.31$	$10232.5 \pm 0.4 \pm 0.5$	–
$M_{\chi_{b1}(nP)}$(MeV)	9893^{+9}_{-11}	10254^{+7}_{-10}	10541^{+24}_{-41}	$9892.78 \pm 0.26 \pm 0.31$	$10255.46 \pm 0.22 \pm 0.50$	$10512.1 \pm 2.1 \pm 0.9$ [12] $10513.42 \pm 0.41 \pm 0.18$ [7]
$M_{\chi_{b2}(nP)}$(MeV)	9923^{+13}_{-14}	10274^{+11}_{-12}	10557^{+22}_{-42}	$9912.21 \pm 0.26 \pm 0.31$	$10268.65 \pm 0.22 \pm 0.50$	$10524.02 \pm 0.57 \pm 0.18$ [7]
$\bar{M}_{nP}$(MeV)	9906^{+8}_{-10}	10263^{+8}_{-11}	10549^{+23}_{-41}	9899.87 ± 0.27	10260.20 ± 0.36	$10530 \pm 5 \pm 9$ [1] $10551 \pm 14 \pm 17$ [2]

Table 8 Differences $\Delta S_n = n^3S - n^1S$. We observe that these differences decrease when n is increased. All the differences reported in this Table are in MeV. These values have been obtained by mean of bootstrap technique. The experimental errors, in the fourth column, has been summed in quadrature

ΔS_n	Theory		Experiment
	Potential I	Potential II	
ΔS_1	53^{+10}_{-18}	51^{+16}_{-13}	61.3 ± 2.3
ΔS_2	18^{+9}_{-10}	17^{+31}_{-5}	24.3 ± 4.5
ΔS_3	11^{+4}_{-31}	11^{+26}_{-4}	–
ΔS_4	8^{+11}_{-54}	8^{+13}_{-3}	–
ΔS_5	6^{+22}_{-67}	6^{+19}_{-8}	–

the impact in the masses of the dynamical effects due to the open bottom thresholds.

4.3 Missing resonances

Besides reproducing the experimentally established states, in Table 5 we provide predictions of states both above and below the open bottom thresholds ($\approx$ 10.6 GeV). In total, we predict 38 states up to 11.3 GeV for 0, 1, 2 (with either $\pm$ combinations for P and C) and 3^{--} quantum numbers. These predicted states are of interest for future analyses at LHCb [15,79,80] and Belle II [13,14,81–83]. In particular, pinning down the $\Upsilon(6S)$ would provide further insight on bottomonium-like states [83].

The missing $\eta_b(nS)$ sector (n^1S_0 states) can be studied through their relation to their angular momentum partners $\Upsilon(nS)$ (n^3S_1) –known from experiment–, by computing the $\Delta S_n = n^3S - n^1S$ mass splitting. This difference should decrease as n increases in the potential model context [84]. The experimental data for ΔS_1 and ΔS_2 shown in Table 8 support this theoretical results. Thereby, we consider our mass estimations for both $\eta_b(nS)$ and $\Upsilon(nS)$ reasonable.

We also provide predictions for states of the $n^{1,3}D_{1,2,3}$ family, which remain undetected except for the 1^3D_2 resonance. The predicted missing states (with uncertainties) provide useful information to guide the forthcoming spectroscopy programs in Belle II [13,14] and LHC [15,16]. However, the production rate of these states should be low, hence, difficult to detect [79].

5 Conclusions

We have developed a relativistic quark model in momentum space to study the bottomonium spectrum. The model closely follows the one used in Ref. [57] to study charmonium. It combines vector and scalar interactions with a momentum dependent screening factor to account for the effects due to virtual pair creation that appear close to the decay thresholds. We fitted our model to all the known states of each J^{PC} below the $B\bar{B}$ threshold except for the recently measured $\chi_{b1}(3P)$ and $\chi_{b2}(3P)$ which we prefer to predict in order to gain insight on their nature and the $\eta_b(2S)$ which we exclude of our fit owing to the disagreement between CLEO and Belle measurements. Our prediction for $\eta_b(2S)$ mass agrees with the Belle result.

We have performed a full statistical error analyses using the bootstrap technique, that provides a rigorous treatment of the statistical uncertainties. In this way we obtain the uncertainties of the parameters and their correlations and we can propagate both to the predicted spectrum. Previous error analyses within phenomenological models have been very limited and incomplete. The rigorous error estimations allow us to assess if the inclusion of a new effect in the phenomenological model is necessary or not, and the correlations provide insight on how independent are the different pieces of the model among them. A full error analyses is mandatory to identify which deviations from experimental data can be absorbed into the statistical uncertainties of the models and which can be related to physics beyond the $b\bar{b}$ picture, guiding future research. We find that the model reproduces very well the fitted states as well as the nonfitted ones within uncertainties.

To asses the importance of a confining term in the scalar interaction, i.e. $\beta_s \neq 0$ in Eq. (7b), we fitted the data with and without such contribution. The results obtained with the two potentials are very similar for the fitted and the predicted states, both in the low and the high parts of the spectrum. Therefore, such confining contribution to the scalar interaction can be disregarded in a bottomonium relativistic model. Even so, the correlations found among the parameters belonging to the scalar interaction and the rest of the model parameters, show that the scalar interaction A in Eq. (7b) is strictly necessary to reproduce the spectrum. The screening factor $F_s(p)$ included in the interaction Hamiltonian begins to impact the predictions in significant way at $\approx$ 11200 MeV, i.e. further away from the open bottom decay thresholds. Hence, the screening effect is not particularly intense and has a slight impact on the bottomonium spectrum, contrary to what it was found for the charmonium one [57].

We have also studied the $\chi_b(3P)$ resonances. In particular we have calculated the mass of each state of this system and its barycenter. The experimental mass value of the $\chi_{b1}(3P)$ falls into the theoretical uncertainty calculated with both potentials. Whereby, we conclude that the model is able to properly predict this state. Also, the model, with both potentials, reproduces the $\chi_{b1}(3P)$ state. Our result indicates that the $\chi_{b1,2}(3P)$ states are more likely to be $b\bar{b}$ mesons than the hypothetical X_b states.

Our model overestimates the $\Upsilon(4S)$ mass and is consistent with results obtained by semirelativistic quark models, within

errors. This is an indication of physics beyond the $b\bar{b}$ picture for this state. We identify the $\Upsilon(10860)$ as a 5^3S_1 state. The model fails to reproduce accurately the $\Upsilon(11020)$, although it was well reproduced by nonrelativistic calculations. Further investigation, within our model, should be performed for this high excitation state.

Finally, we report some states that, up to now, have not been observed experimentally but the confirmation of their existence is part of the experimental plans at LHC B factories and Belle II.

Acknowledgements D.M. thanks Instituto de Ciencias Nucleares (ICN) at Universidad Nacional Autonóma de Mexico for allow the access to the Tochtli-ICN cluster which was used to perform the numerical calculations of this work. This work was supported in part by PAPIIT-DGAPA (UNAM, Mexico) Grant No. IA101819 and CONACYT (Mexico) Grants Nos. 251817 and A1-S-21389. This research was supported by the Munich Institute for Astro- and Particle Physics (MIAPP) which is funded by the Deutsche Forschungsgemeinschaft (DFG, German Research Foundation) under Germany's Excellence Strategy-EXC-2094-390783311.

Data Availability Statement This manuscript has no associated data or the data will not be deposited. [Authors' comment: This work proposes and develops a new theoretical investigation and does not contain experimental data.]

Funded by SCOAP[3].

References

1. G. Aad et al., ATLAS. Phys. Rev. Lett. **108**, 152001 (2012). arXiv:1112.5154 [hep-ex]
2. V.M. Abazov et al., (D0). Phys. Rev. D **86**, 031103 (2012). arXiv:1203.6034 [hep-ex]
3. J. Park (CMS), Proceedings, 46th International Symposium on Multiparticle Dynamics (ISMD 2016): Jeju Island, South Korea, August 29–September 2, 2016. EPJ Web Conf. **141**, 08007 (2017)
4. A.M. Sirunyan et al., (CMS). Phys. Rev. Lett. **122**, 132001 (2019). arXiv:1902.00571 [hep-ex]
5. R. Aaij et al., (LHCb). JHEP **07**, 035 (2019). arXiv:1903.12240 [hep-ex]
6. B.G. Fulsom et al., (Belle). Phys. Rev. Lett. **121**, 232001 (2018). arXiv:1807.01201 [hep-ex]
7. A.M. Sirunyan et al., (CMS). Phys. Rev. Lett. **121**, 092002 (2018). arXiv:1805.11192 [hep-ex]
8. U. Tamponi et al., (Belle). Eur. Phys. J. C **78**, 633 (2018). arXiv:1803.03225 [hep-ex]
9. M. Ablikim et al., (BESIII). Phys. Rev. Lett. **118**, 092002 (2017a). arXiv:1610.07044 [hep-ex]
10. M. Ablikim et al., (BESIII). Phys. Rev. Lett. **118**, 092001 (2017b). arXiv:1611.01317 [hep-ex]
11. S.L. Olsen, T. Skwarnicki, D. Zieminska, Rev. Mod. Phys. **90**, 015003 (2018). arXiv:1708.04012 [hep-ph]
12. M. Tanabashi (Particle Data Group), Phys. Rev. D **98**, 030001 (2018)
13. K. Tanida (Belle II), Proceedings, 13th International Conference on Hypernuclear and Strange Particle Physics (HYP 2018): Portsmouth Virginia, USA, June 24–29, 2018, AIP Conf. Proc. **2130**, 040020 (2019)
14. T.K. Pedlar, Proceedings, 6th International Conference on Exotic Atoms and Related Topics (EXA2017): Vienna, Austria, September 11–15, 2017, EPJ Web Conf. **181**, 01022 (2018)
15. R. Aaij et al. (LHCb), Physics case for an LHCb Upgrade II—Opportunities in flavour physics, and beyond, in the HL-LHC era (2018). arXiv:1808.08865
16. A. Piucci, Proceedings, Workshop on Discovery Physics at the LHC (Kruger2016): Kruger National Park, Mpumalanga, South Africa, December 5–9, 2016. J. Phys. Conf. Ser. **878**, 012012 (2017)
17. F.-K. Guo, C. Hanhart, U.-G. Meißner, Q. Wang, Q. Zhao, B.-S. Zou, Rev. Mod. Phys. **90**, 015004 (2018). arXiv:1705.00141 [hep-ph]
18. R.F. Lebed, R.E. Mitchell, E.S. Swanson, Prog. Part. Nucl. Phys. **93**, 143 (2017). arXiv:1610.04528 [hep-ph]
19. C.-Z. Yuan, Int. J. Mod. Phys. A **33**, 1830018 (2018). arXiv:1808.01570 [hep-ex]
20. Y.-R. Liu, H.-X. Chen, W. Chen, X. Liu, S.-L. Zhu, Prog. Part. Nucl. Phys. **107**, 237 (2019). arXiv:1903.11976 [hep-ph]
21. N. Brambilla, S. Eidelman, C. Hanhart, A. Nefediev, C.-P. Shen, C.E. Thomas, A. Vairo, C.-Z. Yuan, The XYZ states: experimental and theoretical status and perspectives (2019). arXiv:1907.07583 [hep-ex]
22. X. Liao, T. Manke, Phys. Rev. **D65**, 074508 (2002). arXiv:hep-lat/0111049 [hep-lat]
23. S. Meinel, Phys. Rev. D **79**, 094501 (2009). arXiv:0903.3224 [hep-lat]
24. S. Meinel, Phys. Rev. D **82**, 114502 (2010). arXiv:1007.3966 [hep-lat]
25. J.O. Daldrop, C.T.H. Davies, R.J. Dowdall (HPQCD), Phys. Rev. Lett. **108**, 102003 (2012). arXiv:1112.2590 [hep-lat]
26. R. Lewis, R.M. Woloshyn, Phys. Rev. D **85**, 114509 (2012). arXiv:1204.4675 [hep-lat]
27. R.J. Dowdall, C.T.H. Davies, T. Hammant, R.R. Horgan, C. Hughes (HPQCD), Phys. Rev. D **89**, 031502 (2014). arXiv:1309.5797 [hep-lat] [Erratum: Phys. Rev.D92,039904(2015)]
28. C.T.H. Davies, B. Colquhoun, B. Galloway, G.C. Donald, J. Koponen, R.J. Dowdall, R. Horgan, E. Follana, G.P. Lepage, C. McNeile (HPQCD), Proceedings, 31st International Symposium on Lattice Field Theory (Lattice 2013): Mainz, Germany, July 29–August 3, 2013, PoS LATTICE2013, 438 (2014). arXiv:1312.5874 [hep-lat]
29. M. Baker, A.A. Penin, D. Seidel, N. Zerf, Phys. Rev. D **92**, 054502 (2015). arXiv:1504.05979 [hep-ph]
30. H.-T. Ding, O. Kaczmarek, A.-L. Kruse, R. Larsen, L. Mazur, S. Mukherjee, H. Ohno, H. Sandmeyer, H.-T. Shu, Proceedings, 27th International Conference on Ultrarelativistic Nucleus-Nucleus Collisions (Quark Matter 2018): Venice, Italy, May 14–19, 2018, Nucl. Phys. A **982**, 715 (2019). arXiv:1807.06315 [hep-lat]
31. R. Larsen, S. Meinel, S. Mukherjee, P. Petreczky, Phys. Lett. B **800**, 135119 (2020). arXiv:1910.07374 [hep-lat]
32. P. Bicudo, M. Cardoso, N. Cardoso, M. Wagner (2019). arXiv:1910.04827 [hep-lat]
33. R. Larsen, S. Meinel, S. Mukherjee, P. Petreczky, Phys. Rev. D **100**, 074506 (2019). arXiv:1908.08437 [hep-lat]

34. C.S. Fischer, S. Kubrak, R. Williams, Eur. Phys. J. **A51**, 10 (2015). arXiv:1409.5076 [hep-ph]
35. C. Popovici, T. Hilger, M. Gómez-Rocha, A. Krassnigg, Proceedings, Theory and Experiment for Hadrons on the Light-Front (Light Cone 2014): Raleigh, North Carolina, USA, May 26–30, 2014. Few Body Syst. **56**, 481 (2015). arXiv:1407.7970 [hep-ph]
36. T. Hilger, M. Gomez-Rocha, A. Krassnigg, Phys. Rev. D **91**, 114004 (2015). arXiv:1503.08697 [hep-ph]
37. H. Negash, S. Bhatnagar, Adv. High Energy Phys. **2017**, 7306825 (2017). arXiv:1703.06082 [hep-ph]
38. S. Leitão, Y. Li, P. Maris, M.T. Peña, A. Stadler, J.P. Vary, E.P. Biernat, Eur. Phys. J. C **77**, 696 (2017). arXiv:1705.06178 [hep-ph]
39. F.F. Mojica, C.E. Vera, E. Rojas, B. El-Bennich, Phys. Rev. D **96**, 014012 (2017). arXiv:1704.08593 [hep-ph]
40. G.-L. Wan, X.-G. Wu (2019). arXiv:1902.06177 [hep-ph]
41. K. Serafin, M. Gómez-Rocha, J. More, S.D. Głazek, Eur. Phys. J. C **78**, 964 (2018). arXiv:1805.03436 [hep-ph]
42. S.D. Głazek, M. Gómez-Rocha, J. More, K. Serafin, Phys. Lett. B **773**, 172 (2017). arXiv:1705.07629 [hep-ph]
43. S. Godfrey, N. Isgur, Phys. Rev. D **32**, 189 (1985)
44. P. Gonzalez, Phys. Rev. D **80**, 054010 (2009). arXiv:0909.1204 [hep-ph]
45. J.-F. Liu, G.-J. Ding, Eur. Phys. J. C **72**, 1981 (2012). arXiv:1105.0855 [hep-ph]
46. J. Ferretti, E. Santopinto, Phys. Rev. D **90**, 094022 (2014). arXiv:1306.2874 [hep-ph]
47. J. Ferretti, G. Galatà, E. Santopinto, Phys. Rev. D **90**, 054010 (2014). arXiv:1401.4431 [nucl-th]
48. J. Segovia, D.R. Entem, F. Fernández, Phys. Rev. D **91**, 014002 (2015). arXiv:1409.7079 [hep-ph]
49. N. Akbar, M.A. Sultan, B. Masud, F. Akram, Phys. Rev. D **95**, 074018 (2017). arXiv:1511.03632 [hep-ph]
50. W.-J. Deng, H. Liu, L.-C. Gui, X.-H. Zhong, Phys. Rev. D **95**, 074002 (2017). arXiv:1607.04696 [hep-ph]
51. J. Segovia, P.G. Ortega, D.R. Entem, F. Fernández, Phys. Rev. D **93**, 074027 (2016). arXiv:1601.05093 [hep-ph]
52. X.-Z. Weng, L.-Y. Xiao, W.-Z. Deng, X.-L. Chen, S.-L. Zhu, Phys. Rev. D **99**, 094001 (2019). arXiv:1811.09002 [hep-ph]
53. P.K. Srivastava, O.S.K. Chaturvedi, L. Thakur, Eur. Phys. J. C **78**, 440 (2018). arXiv:1806.09348 [nucl-th]
54. A.P. Monteiro, P.P. D'Souza, N. Vidyalakshmi, K.B. Vijaya Kumar, Proceedings, 63rd DAE-BRNS Symposium on Nuclear Physics: Mumbai, Maharashtra, India, December 10–14, 2018, DAE Symp. Nucl. Phys. **63**, 878 (2018)
55. A. Al-Jamel, Mod. Phys. Lett. **2**, 1950307 (2019). arXiv:1908.07707 [hep-ph]
56. B. Chen, A. Zhang, J. He (2019). arXiv:1910.06065 [hep-ph]
57. D. Molina, M. De Sanctis, C. Fernández-Ramírez, Phys. Rev. D **95**, 094021 (2017). arXiv:1703.08097 [hep-ph]
58. S. Dobbs, Z. Metreveli, K.K. Seth, A. Tomaradze, T. Xiao, Phys. Rev. Lett. **109**, 082001 (2012). arXiv:1204.4205 [hep-ex]
59. R. Mizuk et al., (Belle). Phys. Rev. Lett. **109**, 232002 (2012). arXiv:1205.6351 [hep-ex]
60. B.-Q. Li, K.-T. Chao, Commun. Theor. Phys. **52**, 653 (2009). arXiv:0909.1369 [hep-ph]
61. J. Ferretti, G. Galata, E. Santopinto, A. Vassallo, Phys. Rev. C **86**, 015204 (2012)
62. M. De Sanctis, P. Quintero, Eur. Phys. J. A **46**, 213 (2010)
63. J.P. Lees et al., (BaBar). Phys. Rev. D **84**, 072002 (2011). arXiv:1104.5254 [hep-ex]
64. B. Efron, R. Tibshirani, *An Introduction to the Bootstrap, Chapman & Hall/CRC Monographs on Statistics & Applied Probability* (Taylor & Francis, Boca Raton, 1994)
65. R.E. Kass, U.T. Eden, E.N. Brown, *Propagation of Uncertainty and the Bootstrap. In: Analysis of Neural Data* (Springer, New York, 2014), pp. 221–246
66. C. Fernández-Ramírez, I.V. Danilkin, V. Mathieu, A.P. Szczepaniak, Phys. Rev. D **93**, 074015 (2016). arXiv:1512.03136 [hep-ph]
67. J. Landay, M. Döring, C. Fernández-Ramírez, B. Hu, R. Molina, Phys. Rev. C **95**, 015203 (2017). arXiv:1610.07547 [nucl-th]
68. F. James, M. Roos, Comput. Phys. Commun. **10**, 343 (1975)
69. R. Aaij et al., (LHCb). JHEP **10**, 088 (2014). arXiv:1409.1408 [hep-ex]
70. D. Besson et al., (CLEO). Phys. Rev. Lett. **54**, 381 (1985)
71. D.M.J. Lovelock et al., Phys. Rev. Lett. **54**, 377 (1985)
72. D. Santel et al., (Belle). Phys. Rev. D **93**, 011101 (2016). arXiv:1501.01137 [hep-ex]
73. K.F. Chen et al., (Belle). Phys. Rev. Lett. **100**, 112001 (2008). arXiv:0710.2577 [hep-ex]
74. R. Bruschini, P. González, Phys. Lett. B **791**, 409 (2019). arXiv:1811.08236 [hep-ph]
75. C.O. Dib, N. Neill, Phys. Rev. D **86**, 094011 (2012). arXiv:1208.2186 [hep-ph]
76. M.N. Anwar, Y. Lu, B.-S. Zou, Phys. Rev. D **99**, 094005 (2019). arXiv:1806.01155 [hep-ph]
77. M. Karliner, J.L. Rosner, Phys. Rev. D **91**, 014014 (2015). arXiv:1410.7729 [hep-ph]
78. Z.-Y. Zhou, D.-Y. Chen, Z. Xiao, Phys. Rev. D **99**, 034005 (2019). arXiv:1810.03452 [hep-ph]
79. S. Godfrey, K. Moats, Phys. Rev. D **92**, 054034 (2015). arXiv:1507.00024 [hep-ph]
80. Z. Hu, N.T. Leonardo, T. Liu, M. Haytmyradov, Int. J. Mod. Phys. A **32**, 1730015 (2017). arXiv:1708.02913 [hep-ex]
81. B. Fulsom, Proceedings, Meeting of the APS Division of Particles and Fields (DPF 2017): Fermilab, Batavia, Illinois, USA, July 31–August 4, 2017 (2017). arXiv:1710.00120 [hep-ex]
82. H. Ye, Proceedings, 24th International Workshop on Deep-Inelastic Scattering and Related Subjects (DIS 2016): Hamburg, Germany, April 11–15, 2016, PoS **DIS2016**, 262 (2016). arXiv:1607.01740 [hep-ex]
83. W. Altmannshofer et al., (Belle II), The Belle II Physics Book, edited by E Kou and P, Urquijo (2018). arXiv:1808.10567 [hep-ex]
84. S.L. Olsen, Front. Phys. (Beijing) **10**, 121 (2015). arXiv:1411.7738 [hep-ex]